Electronic Supplementary Material (ESI) for ChemComm.

Membrane bound COMT isoform is an interfacial enzyme: general mechanism, new drug design paradigm – Supporting Information

Aniket Magarkar,†§ Petteri Parkkila,† Tapani Viitala,† Tatu Lajunen,† Edouard Mobarak,†,‡ Giuseppe Licari,$ Oana Cramariuc,‡ Eric Vauthey,$ Tomasz Róg,‡,¶ and Alex Bunker*,†

†Drug Research Program, Division of Pharmaceutical Biosciences, Faculty of Pharmacy, University of Helsinki, Helsinki, Finland
‡Department of Physics, Tampere University of Technology, Tampere, Finland
¶ Department of Physics, University of Helsinki, Helsinki, Finland
§ Academy of the Sciences of the Czech Republic, Prague, Czech Republic
$ Department of Physical Chemistry, University of Geneva, 30 quai Ernest-Ansermet, CH-1211 Geneva 4, Switzerland

Contact information: alex.bunker@helsinki.fi

KEYWORDS: molecular dynamics simulation, interfacial enzymes, catechol-O-methyltransferase, drug design, bitopic membrane proteins, lipid membrane interaction, quartz crystal microbalance, , isothermal titration calorimetry, surface plasmon resonance

Contents

Section 1: Molecular dynamics simulations

1.1. Methods

1.1.1 Molecular dynamics potentials for new compounds

Intracellular membrane with COMT inhibitors

Five different COMT inhibitors were simulated interacting with an intracellular membrane, two that are selective for MB-COMT vs. S-COMT, referred to as compound 2 and compound 14, by Robinson *et al.*,[27] and one that was not, compound 8, in addition to entacapone and tolcapone. New potential sets were built for these compounds and all details regarding their construction are provided in the following section.

Parameterization of small molecules:

For all five compounds partial charges were derived in accordance with the OPLS-AA methodology by fitting to the electrostatic potential using the RESP procedure.[1] First the geometry of the compounds was optimized at density functional theory (DFT) level using the Becke B3LYP exchange-correlation functional and the 6-31G* basis set within the Gaussian 03 program.[2] Subsequently, the molecular electrostatic potential was computed for the optimized molecular structure at the same level of theory. The potential obtained through this method was used to calculate the partial atomic charges according to the RESP procedure implemented in ANTECHAMBER.[3] The partial atomic charges are given in **Supporting Information Figure 1**.

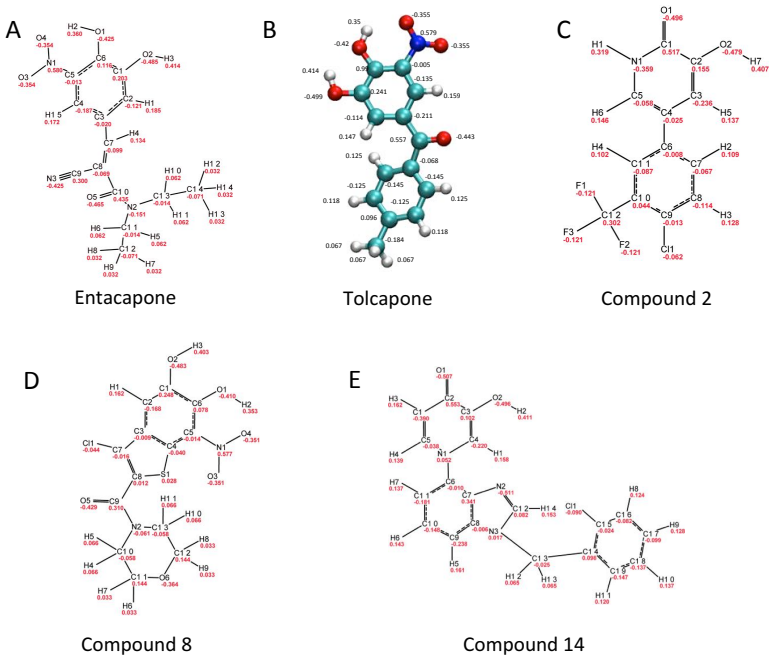

Supporting Information Figure 1: Partial charges for the small molecules

1.1.2 Molecular dynamics simulation for MB-COMT with membrane

Two separate sets of molecular dynamics simulations were performed, intracellular membrane bilayer 1) with MB-COMT selective and non-selective inhibitors and 2) with the entire bitopic MB- COMT protein. Our model of an intracellular membrane bilayer was constructed out of 3 different lipids; 34% DLPC (1,2-dilinoleic-sn-glycero-3-phosphocholine), 56% of DLPE (1,2-dilinoleic-sn-glycero-3-phosphoethanolamine), and 10% DLPS (1,2-dilinoleic-sn-glycero-3-phosphoserine) hydrated with water molecules and Na^+ counter ions added to neutralize the system charge. The membrane bilayer was made up of 128 lipid molecules. For all systems with the COMT inhibitors, 10 inhibitor molecules where placed randomly outside the membrane bilayer in the water, separated from each other. All further details regarding simulated system compositions are given in Supporting Information Table 1.

As shown in Supporting Information Figure 2 of the area per lipid vs. simulation time, and Supporting Information Figure 3 of the Z component of the center of masses of the compounds, the area per lipid equilibrated after 60 ns in all systems. The Z components of compounds 2, 8 and 14 had also equilibrated after 60 ns. For the system with entacapone, however, the equilibration of this property was seen to have been achieved after 120 ns. For all systems we continued the simulation for 100 ns beyond the equilibration time and made our analysis based on these results.

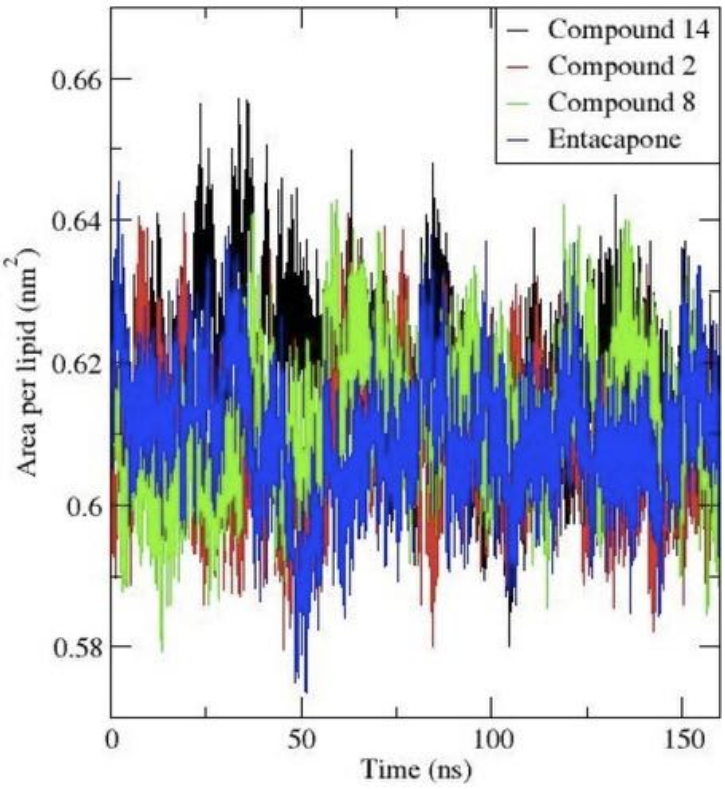

Supporting Information Figure 2: Area per lipid vs. simulation time. All systems have reached an equilibrium area per lipid after approximately 60 ns.

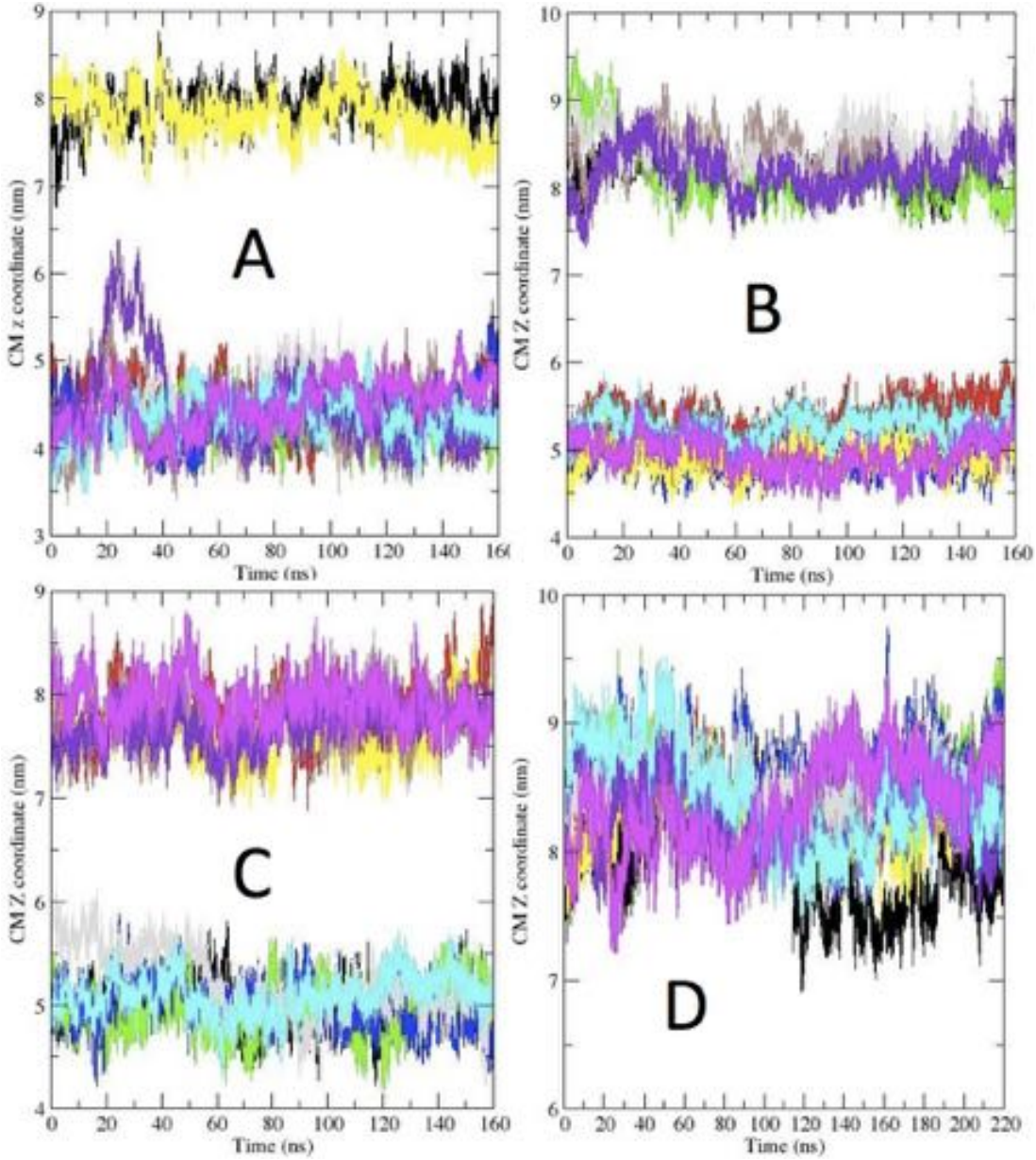

Supporting Information Figure 3: Z component (component along membrane normal) of the center of mass of the four compounds throughout the simulation. (A) Compound 2 (B) Compound 8 (C) Compound 14 and (D) Entacapone. These results indicate that all systems have reached equilibrium. The different colours correspond to the trajectories of different individual molecules.

Intracellular membrane with MB-COMT protein

The structure for the 26 residue linker attached to a 24 residue long transmembrane alpha helix segment was taken from a previous study.[4] In this study, this structure was derived from extensive replica exchange molecular dynamics simulations in conjunction with the optimized potential for efficient structure prediction. Six independent sets of simulations of a transmembrane

helix in membrane bilayers were performed, starting from a range of initial conformations, which converged to produce structures with similar interaction features. For our current simulation of the entire MB-COMT enzyme bound to an intracellular membrane, we used, as the starting point of the simulation, two configurations obtained in the aforementioned study.[4] We added the catalytic domain of the protein in both apo and holo forms (two different structures) using structures for S-COMT in both forms determined through X-ray crystallography, PDB structures 2ZLB [5] for the apo form and 2CL5 [6] for the holo form. We first performed MD simulation with the protein motion constrained for 100 ns to equilibrate the membrane around the protein. We then performed another MD simulation with only the catalytic domain restrained for 50 ns, and finally removed all restraints and simulated for another 100 ns to attain an initial equilibrium configuration. We then performed three separate 500 ns simulations for each of the two initial structures, for a total ofsix simulations.

System	1	2	3	4	5	6	7	8	9	10	11
DLPC	44	44	44	44	98	98	98	98	98	98	98
DLPE	60	60	60	60	132	132	132	132	132	132	132
DLPS	24	24	24	24	52	52	52	52	52	52	52
Comp. 2	10	-	-	-	-	-	-	-	-	-	-
Comp. 8	-	10	-	-	-	-	-	-	-	-	-
Comp. 14	-	-	10	-	-	-	-	-	-	-	-
Entacap.	-	-	-	10	-	-	-	-	-	-	-
Tolcapone	-	-	-	-	-	-	1	-	-	-	-
MB-COMT	-	-	-	-	1	1	-	-	-	-	-
ADOMET	-	-	-	-	-	1	-	-	1	1	-
S-COMT	-	-	-	-	-	-	-	1	1	-	-
Water	10924	10924	10924	10924	33121	33121	10924	33121	33121	10924	10924
Mg2+	-	-	-	-	-	-	-	-	-	-	24

Supporting Information Table 1: Composition of simulation systems

1.1.3 Molecular dynamics simulation for S-COMT with membrane

Umbrella sampling to obtain PMF of S-COMT with membrane bilayer

The initial simulations for S-COMT in apo and holo forms were performed using the same methodology as for MB-COMT (see above). The free-energy calculations were performed using the umbrella sampling protocol implemented in GROMACS. The initial structures for umbrella sampling were taken from the equilibrated simulation trajectory for the apo-protein with membrane, holo-protein with membrane and ADOMET with membrane simulations. The pull rate for the initial pulling was 0.001 Å/ps, and the force constant for the pulling was 10 kJ mol^{-1} $Å^{-2}$. The reaction coordinate was the distance between the center of mass of the protein/ADOMET and membrane. The simulations in each umbrella window were 100ns long. The free-energy profiles, calculated using the weighted histogram analysis method (WHAM), in addition to all error estimates, determined from a bootstrap analysis based on generating bootstrapped trajectories from the umbrella histograms, were performed according to the protocol described by Hub et al.[7]

Section 2: Surface Second Harmonic Generation:

2.1 Methods

Stock solutions of the dyes were prepared in DMSO (Acros Organics, spectroscopic grade) at 2.5 mM concentration. For the SSHG experiments, aqueous solutions of 10μM concentration were freshly prepared from the stock. Dodecane (DOD, 99+%) was purchased from Alfa Aesar. POPC (1-palmitoyl-2-oleoyl-*sn*-glycero-3-phosphocholine, P3017), tolcapone (SML0150) and entacapone (SML0654) were purchased from Sigma-Aldrich. POPE (1-palmitoyl-2-oleoyl-sn-glycero-3-phosphoethanolamine, 850757P) and POPS (1-palmitoyl-2-oleoyl-sn-glycero-3-phospho-L-serine (sodium salt), 840034P) were obtained from Avanti Polar Lipids. A Stock solution of 1mM in chloroform containing a mix of the three phospholipids (POPC:POPE:POPS in molar ratio 11:15:6) was used for the preparation of the monolayer.
The SSHG experiments were performed at the dodecane/phospholipid monolayer/water interface. The presence of the dodecane in the upper phase is needed in order to have the total internal reflection condition, which enhances by far the detected second-harmonic signal. The samples were prepared by pouring 10 ml of aqueous solution of tolcapone or entacapone into a 4x4x4 cm^2 quartz cell, spreading a certain amount of phospholipid mixture to have an area per lipid of about 60 $Å^2$, waiting for the chloroform to evaporate and then adding slowly 12 ml of dodecane.
Steady-state absorption spectra were recorded on a Cary 50 spectrophotometer (Varian) using 1 cm quartz cells. The experiments were performed at 20 ± 1 °C.

2.2 *Surface Second Harmonic Generation experiments*

The SSHG setup has been described in detail previously. [8,9]. The probe pulses (~100 fs, ~1.5 μJ) at three different wavelengths (800, 860 and 920 nm) were generated by a collinear optical parametric amplifier (TOPAS-C, Light Conversion) pumped by the output of a Ti:Sapphire amplifier (Solstice, Spectra-Physics) and focused onto the sample by a 400 mm lens. The total internal reflection condition was achieved using an angle of incidence of about 70°. No signal coming from the dodecane/monolayer/water interface without dye could be detected. The polarization of the probe beam was scanned using a half-wave plate, whereas the *p* (0°), *s* (90°) or 45° polarisation components of the second-harmonic signal were selected using a wire-grid polariser (data reported in **Supporting Information Figure 11**).
The nonlinear SSHG intensity at the frequency 2ω under total internal reflection condition can be expressed as: [10,11]

$$I_{SSHG} = \frac{\omega^2}{8\varepsilon_0 c^3} \frac{\left(\varepsilon_1^{2\omega}\right)^{1/2}}{\varepsilon_1^{\omega}\left(\varepsilon_m^{2\omega} - \varepsilon_1^{\omega}\sin^2\theta_1^{\omega}\right)} \left|\chi^{(2)}\right|^2 I_{pr}^2 \quad \textbf{(eq. 1)}$$

where $\varepsilon_{1,m}^{\omega}$ and θ_1^{ω} are the relative dielectric constants and the angle of incidence of the probe beam at ω. Here, the subscripts *1* and *m* refer to the upper dodecane phase and the dodecane/phospholipid/water interface, respectively. The macroscopic nonlinear optical susceptibility, $\vec{\chi}^{(2)}$, is a second rank tensor

containing 27 elements. However, in the case of isotropic interfaces, it contains only seven nonzero elements, three of which are independent. The dependence of the SSHG intensity polarized at Γ on the polarization of the probe field, γ, is given by:

$$I_{SSHG}(\gamma,\Gamma) = C\left|a_1\chi^{(2)}_{XXZ}\sin 2\gamma \sin\Gamma + \left(a_2\chi^{(2)}_{XXZ} + a_3\chi^{(2)}_{ZXX} + a_4\chi^{(2)}_{ZZZ}\right)\cos^2\gamma\cos\Gamma + a_5\chi^{(2)}_{ZXX}\sin^2\gamma\cos\Gamma\right|^2 I^2_{pr} \quad \textbf{(eq. 2)}$$

where the a_1-a_5 coefficients (listed in **Supporting Information Table 2**) are determined from the refractive indices of the different media and the angle of incidence. These coefficients were calculated as described in ref.[3] using the following values:

$$n_{1,dod} = 1.42; \quad n_{2,wat} = 1.33; \quad n_m = 1.378$$

where n_m was calculated as the average of n_1 and n_2.[12] Moreover no dispersion was assumed, i.e. the frequency dependence of the refractive indices was neglected.

Coefficients	*Real part*	*Imaginary*
a_1	5.37972	-5.84029
a_2	0.05387	-0.0627639
a_3	-0.026935	0.0313819
a_4	4.86507	-5.66829
a_5	5.37972	-5.84029

Supporting Information Table 2. Coefficients determined from the refractive indices of the different media and the angle of incidence.

A global fit of equation 2 to the set of three polarization-resolved SSHG data (Γ = *p*, *s* and 45°) gives the ratios of the macroscopic susceptibility elements reported in **Supporting Information Table 3**.

A quantitative comparison between the polarization-resolved SSHG data and the simulations was not attempted as a result of several factors: a) the error on the determination of the non-linear optical susceptibility for entacapone is large due to the fact that the second-harmonic signal at the *s* polarization is close to zero (see **Supporting Information Figure 11**); b) the distributions of orientation for both entacapone and tolcapone extracted from the MD trajectories are broad and can be reproduced only using several Gaussian functions, while the SSHG experiments give a single average distribution angle. Moreover, c) the hyperpolarizability tensor of the two compounds is dominated by more than one single element; this complicates the analysis of the data (**Supporting Information Figure 14**).

Section 3: Quartz Crystal Microbalance, Surface Plasmon Resonance and Isothermal Titration Calorimetry

3.1 Materials and Methods

3.1.1 Materials

NaCl (sodium chloride, 71382), NaOH (sodium hydroxide, 71690), $CaCl_2$ (calcium chloride, C4901), H_2O_2 (hydrogen peroxide solution, 30 wt % in H_2O, H3410), NH_4OH (ammonium hydroxide solution, 28-30% NH_3 basis, 320145), HEPES (4-(2-hydroxyethyl)-1-piperazineethanesulfonic acid, H3375) and ADOMET (S-(5'-Adenosyl)-L-methionine chloride dihydrochloride, A7007) were obtained from Sigma-Aldrich (Helsinki, Finland). S-COMT (catechol-O-methyl transferase) was either from porcine liver (Sigma-Aldrich, C1897) or from human (a kind gift from Orion Oyj, Espoo, Finland). DOPC (1,2-dioleoyl-sn-glycero-3-phosphocholine, 25 mg/ml in $CHCl_3$, 850375C), DOPE (1,2-dioleoyl-sn-glycero-3-phosphoethanolamine, DOPE, 10 mg/ml in $CHCl_3$, 850725C), DOPS (1,2-dioleoyl-sn-glycero-3-phospho-L-serine (sodium salt), 10 mg/ml in $CHCl_3$, 840035C) and CHAPS (3-[(3-) cholamidopropyl) dimethylammonio]-1-propanesulfonate, 850500) were obtained from Avanti Polar Lipids (Alabaster, USA). Ethanol (95%) was obtained from Altia Corp. (Rajamäki, Finland). Hellmanex II was obtained from VWR Finland (Helsinki, Finland).
Ion exchanged water for the preparation of water based solutions and buffers used in all experiments was obtained from a Milli-Q purification system providing water with a resistivity of 18 MΩ cm and a TOC level of < 5 ppm. SiO_2 coated 5 MHz quartz crystal sensors for quartz crystal microbalance (QCM) measurements were obtained from Q-Sense/Biolin Scientific (Västra Frölunda, Sweden), and SiO_2 coated gold sensors for surface plasmon resonance measurements (SPR) were obtained from Bionavis Ltd (Tampere, Finland).

3.1.2 Techniques for interaction measurements with supported lipid bilayers and vesicles

Two surface-sensitive label-free techniques, i.e. quartz crystal microbalance (QCM) and surface plasmon resonance (SPR), were used to monitor the interaction of COMT, ADOMET and a mixture of these (COMT+ADOMET) with supported lipid bilayers (SLBs) prepared from DOPC:DOPE:DOPS vesicles (QCM experiments) or DOPC vesicles (SPR experiments). Additionally, isothermal titration calorimetry (ITC) was used to measure the interaction of COMT, ADOMET and COMT+ADOMET with DOPC:DOPE:DOPS vesicles.

The impedance-based QCM instrument (QCM-Z500, KSV Instruments Ltd, Helsinki, Finland) used in this study measures the changes in the oscillation frequency and dampening of the oscillation of a disk-shaped quartz crystal resonator at multiple overtone frequencies upon adsorption/desorption of material at the sensor surface. The oscillation frequency of the quartz crystal sensor is decreased/increased when mass adsorbs/desorbs on/from the sensor surface. The dampening, i.e. dissipation, of the quartz crystal sensor oscillation reflects the viscoelastic properties of the mass coupled to the sensor surface.

The two-channel multi-parametric surface plasmon resonance instrument (BioNavis 220A, BioNavis Ltd, Tampere, Finland) was used as a complementary method to QCM. The multi-parametric instrument used in this study measures the relative intensity of reflected p-polarized light from the sensor surface over a wide range of incident angles (30-80°). This allows the determination of the full SPR spectra as a function of time. Adsorption/desorption of molecules on the sensor surface induces an increase/decrease in the SPR peak angular position which is monitored in real-time during the measurements. In addition, the contribution of the optical properties of the running buffer on the SPR peak angular position can be eliminated by exploiting the angle of total internal reflection which is an integral part of the full SPR spectra recorded. This ensures that the obtained SPR signal response is only originating from the interactions taking place on the sensor surface.
A MicroCal VP-ITC instrument (Malvern Instruments, Malvern, United Kingdom) was used for the isothermal titration calorimetry measurements. The ITC instrument measures the affinity and thermodynamics of biomolecular interaction events by directly measuring the heat released or absorbed during a binding event.

3.1.3 Vesicle preparation

Vesicles were formed by the thin film hydration method followed by either sonication (for QCM measurements) or extrusion through a polycarbonate membrane (for SPR and ITC measurements). The lipids dissolved in chloroform were first mixed in a glass tube in molar ratios of 11:15:6 (DOPC:DOPE:DOPS, for QCM and ITC measurements) or as pure DOPC (for SPR measurements). The tube was then placed in a water bath within a larger glass tube and attached to a vacuum rotary evaporation system (Büchi R-114, Büchi Labortechnik AG, Flawil, Switzerland). Chloroform was evaporated by heating the tube to 60 °C and gradually reducing the pressure to 70 mbar under a nitrogen flow. The resulting thin lipid layer was hydrated with 1 mL of HEPES buffer (20 mM HEPES, 140 mM NaCl, pH 7.4) by gently stirring the tube in a water bath (60 °C) for 1 h. For QCM measurements the hydrated lipid solution was sonicated with an Elmasonic S 40 H sonicator (Elma Schmidbauer GmbH, Singen, Germany) to form the vesicle solution. The particle size of the vesicles for QCM measurements was 55 ± 3 nm, number size distribution (determined by using a Zetasizer Nano Z instrument, Malvern UK). For ITC and SPR measurements the hydrated lipid solution was extruded at 60°C through a polycarbonate membrane using a syringe extrusion device (Avanti Polar Lipids). After the extrusions, the vesicle solution was quickly cooled down and stored in a refrigerator. Vesicles extruded only through a 200 nm membrane were used for ITC measurements and exhibited a particle size of 128 ± 38 nm (determined using a Zetasizer APS dynamic light scattering automated plate sampler, Malvern Instruments, Malvern, United Kingdom). Smaller vesicles with a diameter < 100 nm were used for SPR measurements. For this, the hydrated vesicle sample was first extruded 11 times through a 100 nm pore sized membrane followed by 11 extrusions through a 50 nm pore sized membrane. The particle size of the vesicle solution used in all SPR measurements was 62 ± 17 nm (determined by using a Zetasizer APS dynamic light scattering

automated plate sampler, Malvern, United Kingdom). The total lipid concentration of the stock vesicle solutions were 13 mM. The vesicle stock solutions were stored at +4 ◦C and used within four weeks from preparation.

3.1.4 Formation of supported lipid bilayers for QCM and SPR measurements

3.1.4.1 QCM

The SiO_2 coated quartz crystal sensor used as a support for forming the SLBs was initially cleaned by immersing the crystal in a boiling solution of 1:1:5 H_2O_2:NH_4OH:H_2O by volume ratio for ten minutes, then flushing it with copious amounts of ion exchanged water followed by blowing it dry with nitrogen gas. The clean SiO_2 coated quartz crystal sensor was then placed into the flow channel of the QCM instrument and the flow channel was filled with the running buffer and left to stabilize for 20 minutes at 20°C while continuously flushing running buffer (HEPES buffer; 20 mM Hepes, 150 mM NaCl, pH 7.4) through the flow channel at a flow speed of 250 µl/min. The formation of the SLB was verified and monitored by recording the frequency change and dissipation change at the 3rd, 5th, 7th, and 9th overtones. Experiments were performed by 1) measuring a baseline with the running buffer for ca. 10 minutes, 2) injecting a DOPC:DOPE:DOPS vesicle solution (0.2 mg/mL of total lipids) diluted from the stock vesicle solution with HEPES buffer containing 5 mM $CaCl_2$ into the QCM flow channel for 5 minutes, 3) rinsing the QCM flow channel for 5 minutes with the running buffer, and 4) reducing the flow speed of the running buffer to 50 µl/min. After reducing the flow speed in the QCM flow channel a 15 minute stabilization period was allowed before injecting samples of ADOMET, COMT or (COMT+ADOMET) for monitoring the interaction with the SLB. The SiO_2 quartz crystal sensor was washed in situ in the flow channel after each interaction measurement with sequential five minute injections of 20 mM CHAPS, 2% Hellmanex II, 95% ethanol, and ultrapure H_2O. This allowed for the immediate preparation of a new fresh SLB on the same SiO_2 quartz crystal sensor for each interaction measurement with ADOMET, COMT or (COMT+ADOMET).

3.1.4.2 SPR

The SiO_2 coated SPR sensors were initially washed with ethanol and ultrapure H_2O, dried with nitrogen, and cleaned from organic contaminants using oxygen plasma for 5 minutes. Hereafter, a baseline was measured for at least 5 min at 20°C with the running buffer flowing through the SPR flow channel at a flow speed of 30 µl/min. Then, a DOPC vesicle solution (0.15 mg/mL of total lipids), diluted from the stock vesicle solution with HEPES buffer containing 5 mM $CaCl_2$, was injected into the SPR flow channel with a flow speed of 20 µl/min. The injection time for the vesicle solution was 5 minutes followed by subsequent injections of calcium-free buffer and ultrapure H_2O to ensure complete surface saturation which induces vesicle rupture and SLB formation. The flow speed was then reduced to 7 µl/min for interaction measurements of ADOMET, COMT or (COMT+ADOMET) with the SLB. After each experiment, the cleaning process was repeated along with an additional initial wash with 20 mM CHAPS to ensure complete removal of lipids from the SiO_2 coated SPR sensor surface.

3.1.5. Interaction measurements of ADOMET, COMT and (COMT+ADOMET) with SLBs and vesicles

The interaction between ADOMET, COMT and (COMT+ADOMET) with the DOPC:DOPE:DOPS SLB was monitored in situ with the QCM by recording the frequency change and dissipation change at the 3rd, 5th, 7th, and 9th overtones during 10 minute injections of either 2 mM ADOMET, 40 μM COMT or (2 mM ADOMET+40 μM COMT). COMT from porcine liver was used in the QCM measurements.
The same concentrations were used in the SPR measurements. The change in the SPR peak angular position was measured with a laser wavelength of 670 nm during 10 minute injections of either 2 mM ADOMET, 40 μM COMT or (40 μM COMT+2 mM ADOMET). Any bulk contributions from the samples to the measured SPR responses were eliminated by using the Data Viewer software (version 4.2.5) provided by BioNavis Ltd (Tampere, Finland). COMT from human was used in the SPR measurements. The QCM and SPR measurements were repeated three times. One-way analysis of variance (ANOVA) was used for statistical analysis.

3.1.6 ITC

For ITC measurements all solutions were first thoroughly degassed prior to the experiments. Then, either 4 μM COMT, 0.2 mM ADOMET, or (4 μM COMT+0.2 mM ADOMET) were placed in the sample cell. The temperature was allowed to stabilize to 37°C, whereafter 5 μL of the vesicle solution (total lipid concentration of 5 mM) was injected repeatedly into the sample cell under continuous stirring while simultaneously recording the heat flow. The analysis of the ITC measurements were performed by determining the area of the injection heat pulses to generate the titration curves for extraction of the thermodynamic parameters (AFFINImeter, S4Sd, Santiago de Compostela, Spain). The human form of COMT was used in all ITC measurements. The ITC measurements were performed once. The error bars for the ITC measurements were provided by the AFFINImeter software and are error estimates of the fitting to the measured data.

Section 4: Molecular dynamics simulations results

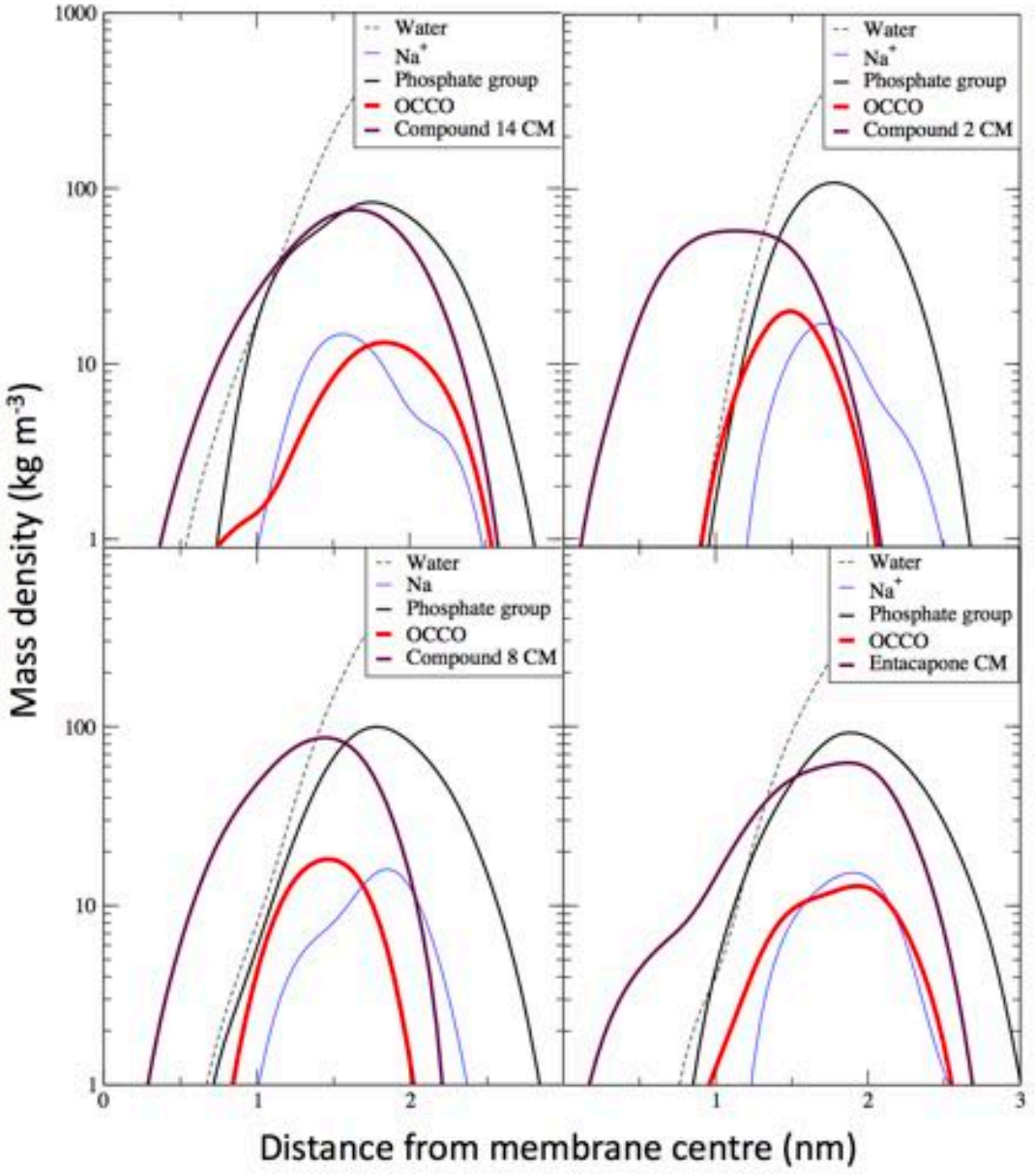

Supporting Information Figure 4: Mass density as a function of distance from the membrane center of both the center of mass of the entire compound and the OCCO (catechol) group. The value of this quantity for the Na^+ ions and phosphate headgroup peak are shown for reference.

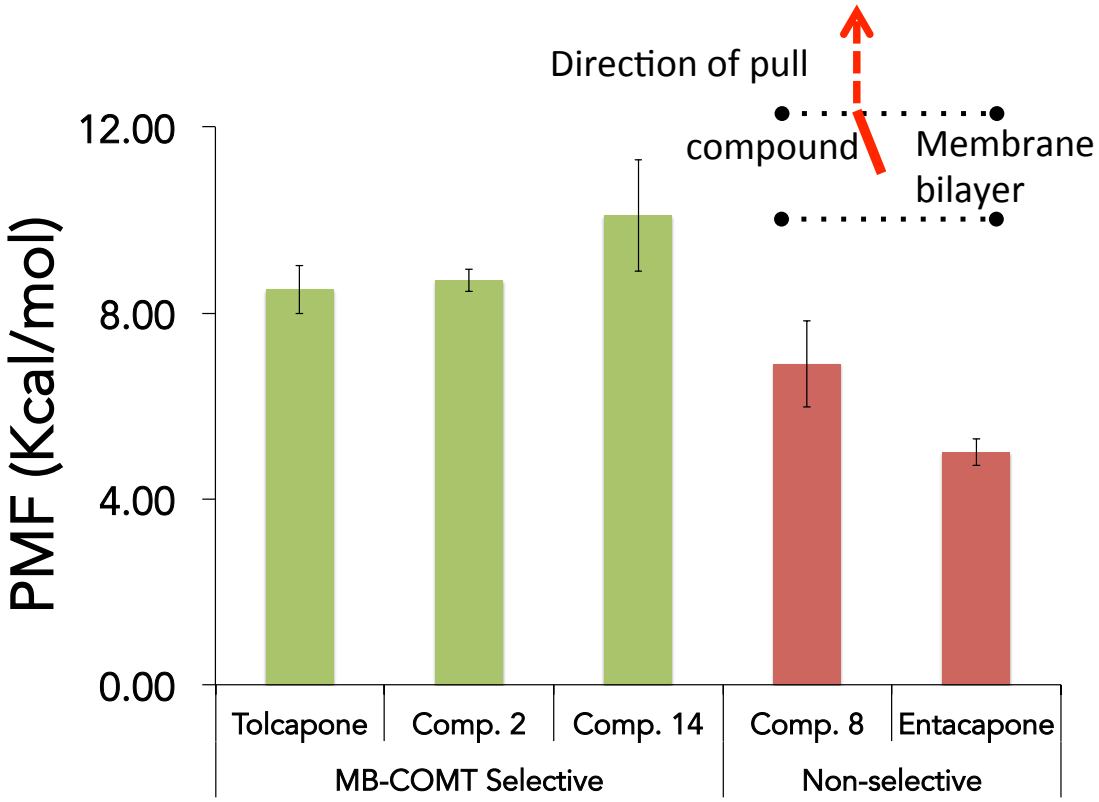

Supporting Information Figure 5: Potential of mean force to pull molecule out of the membrane bilayer.

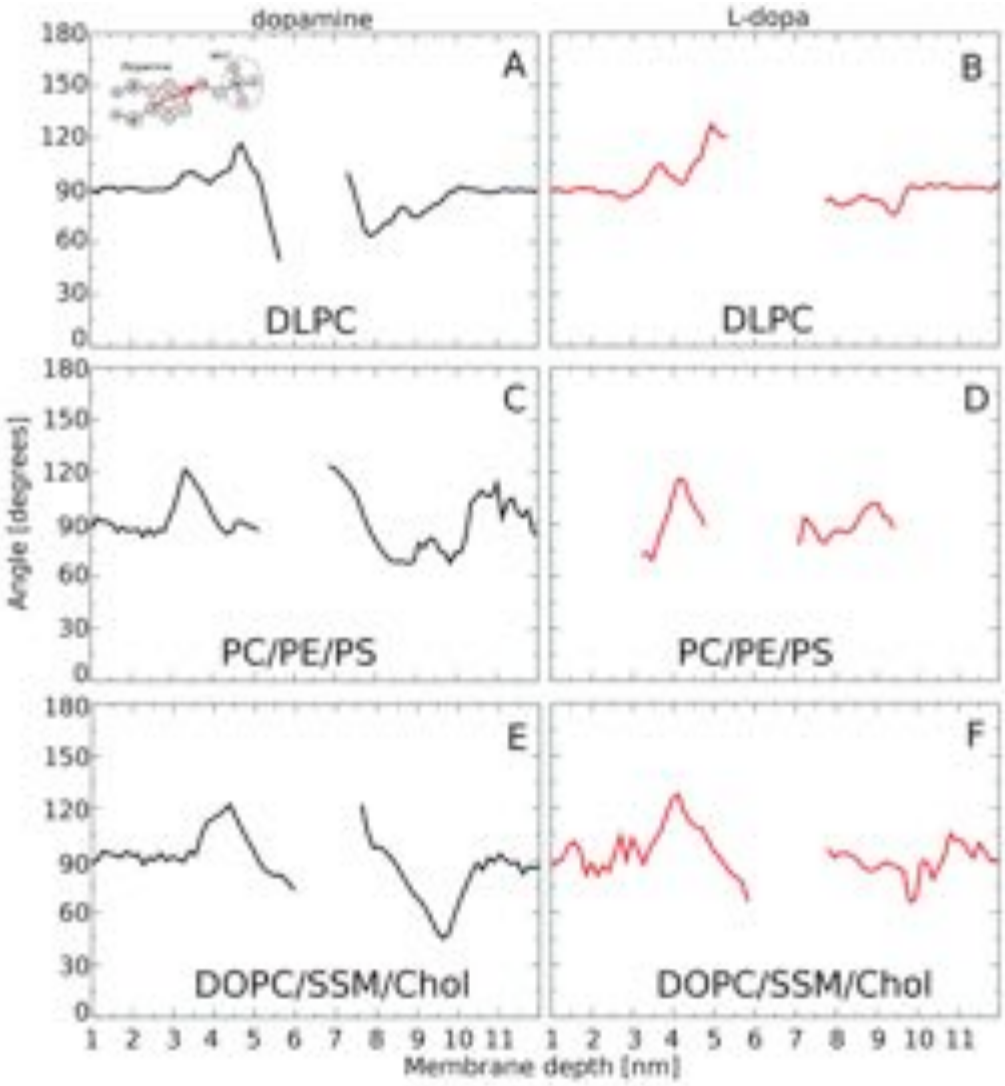

Supporting Information Figure 6: Average angle between the vector CB-CZ and the bilayer normal. The breaks in the curve reflect the lipid bilayer core, where dopamine and L-dopa do not penetrate. Bilayers were composed of 128 molecules of dilineoylphosphatidylcholine (DLPC, di-18:2-DLPC; DLPC bilayer) panel a and b; 44 DLPC, 60 dilineoylphosphatidylethanolamine (DLPE, di-18:2-PE) and 24 dilineoylphosphatidylserine (DLPS, di-18:2-PS) molecules (PC/PE/PS bilayer) panel c and d; 48 sphingomyelin (SM), 48 dioleoylphosphatidylcholine (DOPC), and 32 cholesterol molecules (DOPC/SSM/CHOL bilayer) panel e and f.

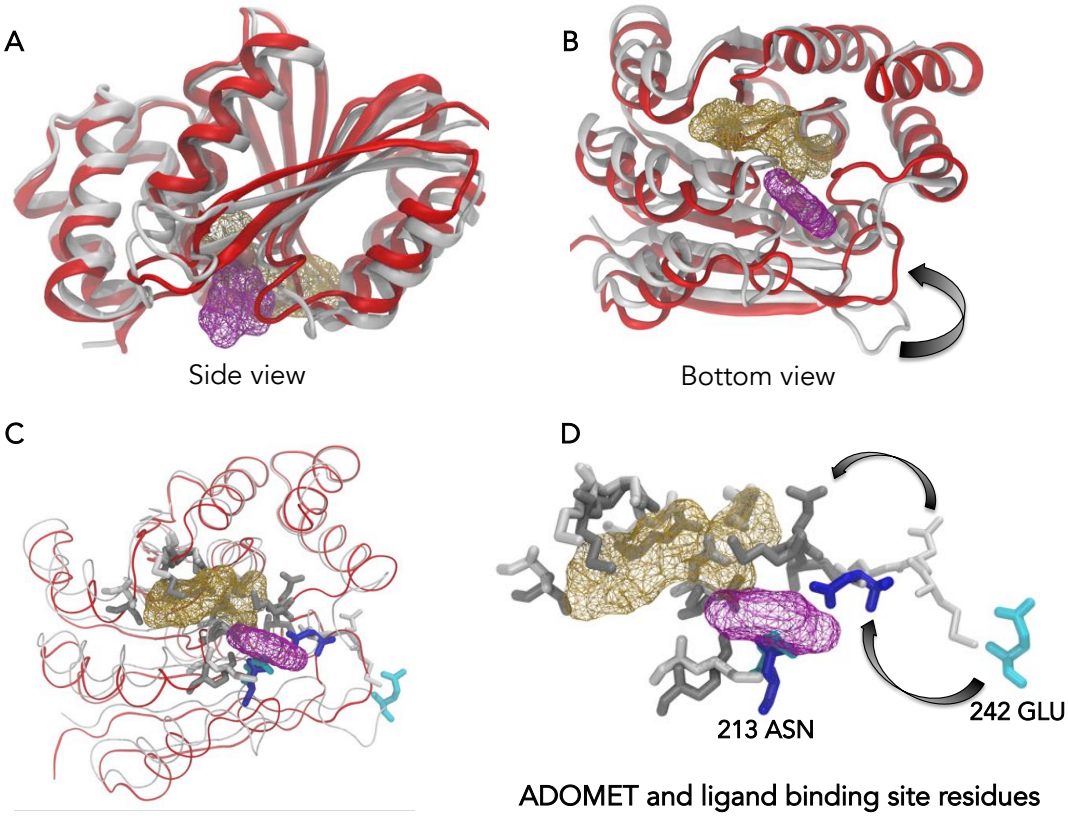

Supporting Information Figure 7: Comparison of the apo and holo forms of the structure of the catalytic domain of COMT. The structures used for analysis were taken from configurations obtained from MD simulation once equilibrium was obtained. We show the superposition of the apo and holo forms, shown in white and red respectively, from two separate perspectives "side" (A) and "bottom", the catalytic surface, (B). The ADOMET binding site is shown in gold space-fill representation and the ligand-binding site is shown in violet space-fill representation. The RMSD between the apo and holo forms of the protein is 2.94 Å. Observing the "bottom view" (B) we see the movement of a key loop, indicated by the grey arrow, in the presence of ADOMET. In (C) we show residues in the ADOMET binding site, shown in white and gray, for the apo and holo forms respectively and the substrate binding site residues are shown in light blue and dark blue, for the apo and holo forms respectively. In (D) we present a closer look at the interactions between ADOMET and the ligand for both the apo and holo forms of COMT.

From previous structural and bio-physical studies it is known that the Apo form of COMT has no cleft corresponding to the ADOMET binding site, and the structure is defined as a "partially open form". The substrate recognition site where the drug binds is not clearly defined [5], this is due to the fact that, the ligand binding site residue GLU242 is located in the loop region, which is flexible in the apo form as shown in our simulation studies. Upon the binding of ADOMET, this loop region is brought closer to the residue 213ASN, this in turn defines the ligand-binding site. These structural changes in the protein bring about, 1) the increase in the accessible hydrophobic surface area of the protein

as shown in **Supporting Information Figure 9A**, 2) a decrease in the accessible hydrophobic surface area as the protein interacts with the membrane (shown in **Supporting Information Figure 10B**) showing that it is buried in the membrane and 3) an increase in the number of hydrogen bonds between the protein and membrane lipids (shown in **Supporting Information Figure 10C**).

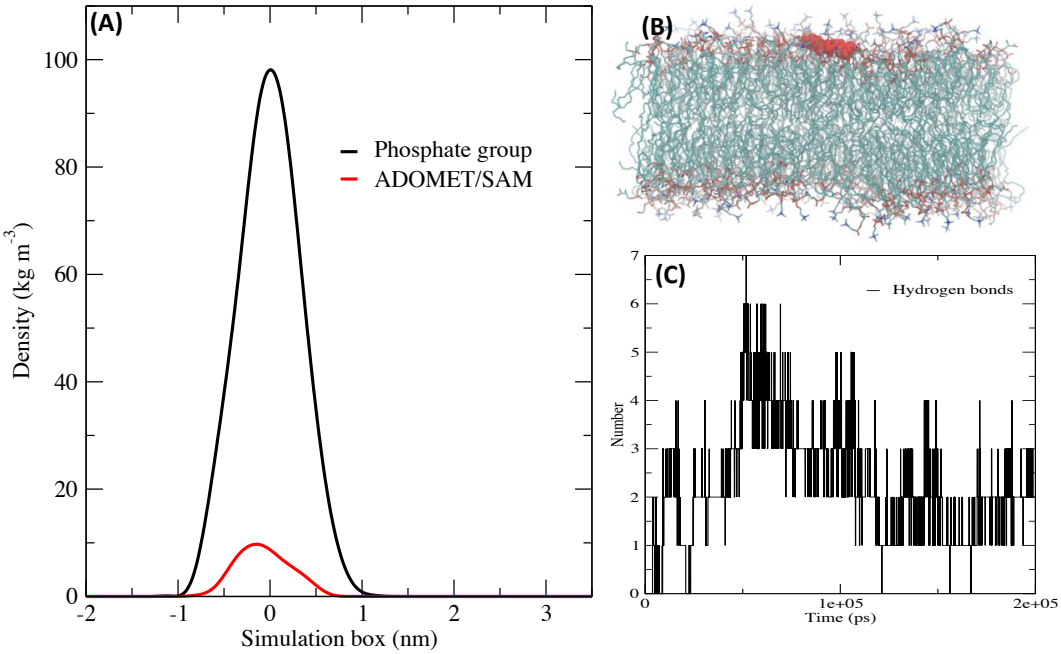

Supporting Information Figure 8: Interaction of ADOMET with membrane bilayer. (A) Mass density profile and (B) Simulation snapshot for the interaction of membrane with ADOMET (ADOMET is shown in red. Both Mass density profile and snapshot shows that the ADOMET collocates with the membrane headgroups. (C) Number of hydrogen bonds between ADOMET and membrane. When dopamine is located higher in the membrane, closer to the water phase, the catechol group is oriented outwards from the membrane, towards the water phase, in a similar fashion to MB-COMT selective inhibitors. When it is located deeper in the membrane, however, the molecule reverses orientation. Since dopamine molecules located closer to the water phase are more accessible to the enzyme their orientation is optimal for interaction with COMT.

A

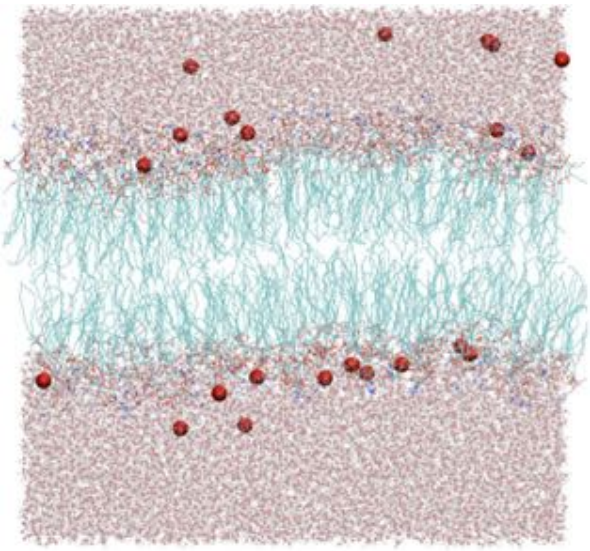

B

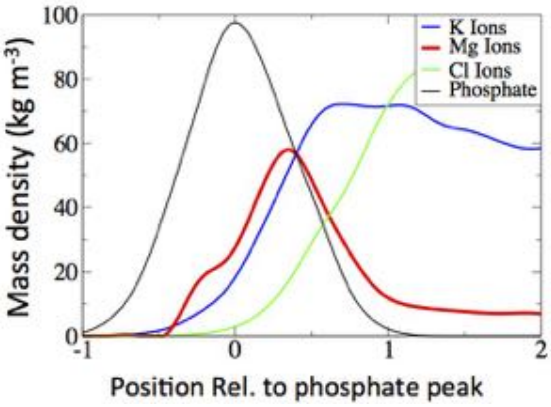

Supporting Information Figure 9: (A) Snapshot of the simulations of Mg^{2+} ions with membrane bilayer (B) Mass density profile and snapshot showing affinity of Mg^{2+} ions for the membrane headgroups.

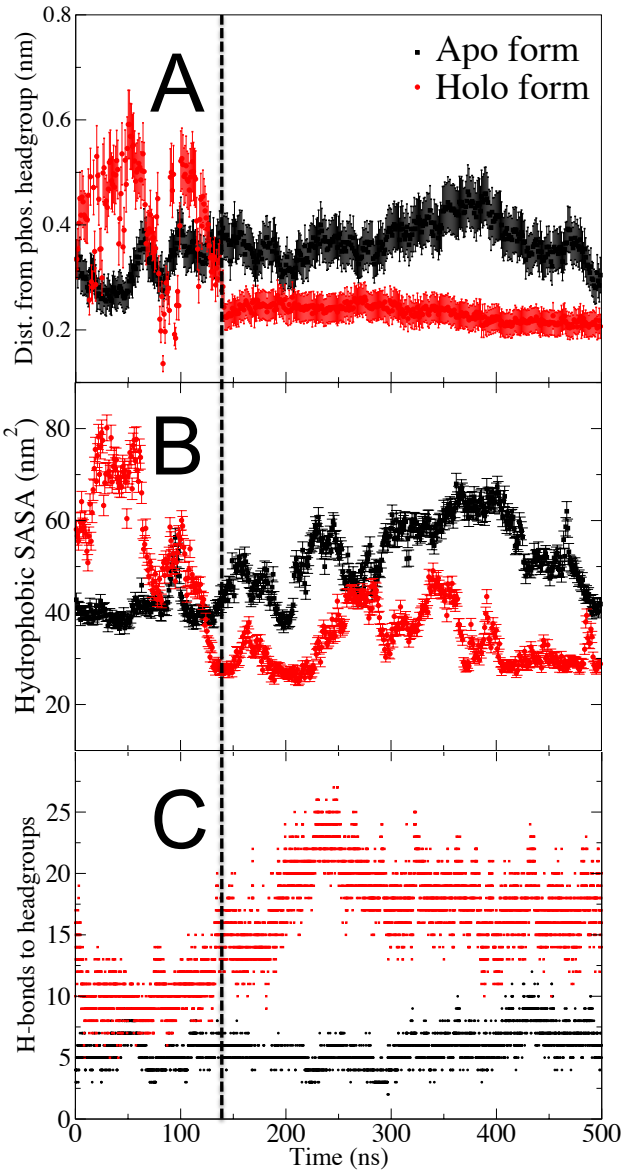

Supporting Information Figure 10. Plots of measurable quantities as a function of simulation time that indicate the binding to the membrane of the Holo form of MB-COMT. The vertical dotted line indicates the time at which the active site of the protein was observed to firmly attach to the membrane surface. (A) The distance perpendicular to the membrane normal of the active site from the phosphate headgroup, (B) the hydrophobic solvent accessible surface area (SASA) and (C) The number of H-bonds between the catalytic domain of MB-COMT and the membrane headgroups.

Section 5: Results – SSHG experiments and DFT calculations

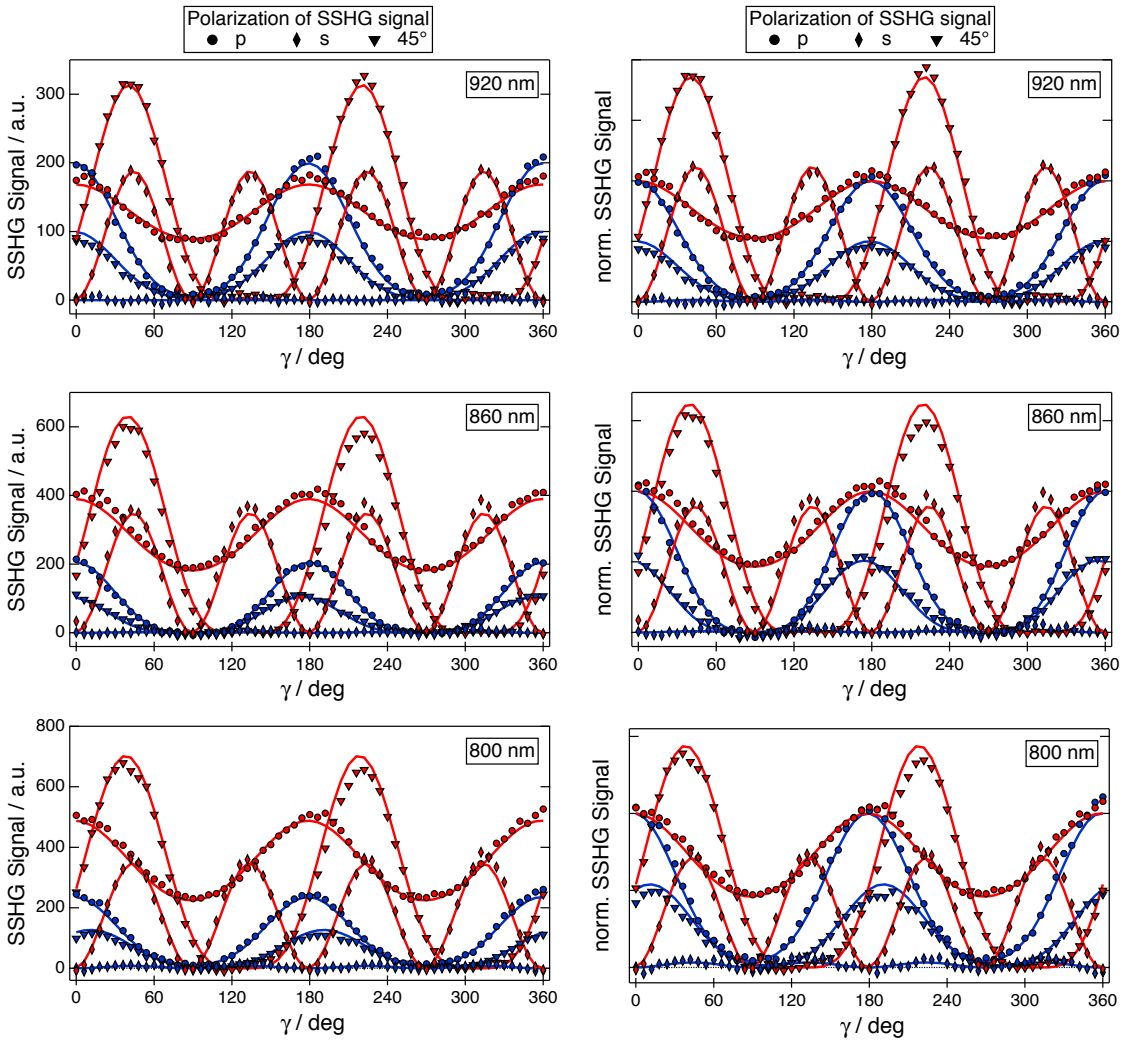

Supporting Information Figure 11: Polarization-resolved SSHG curves for tolcapone (red) and entacapone (blue) at three different probing wavelengths. Three components of the SSHG polarization are shown (Γ = *p* (circles), *s* (diamonds) and 45° (triangles)) as a function of the probe polarization (γ). The absolute values of the SSHG signal are reported on the left column whereas the normalized signal to the maximum of the fit *p* curve is reported on the right column.

	Wavelength	$\chi^{(2)}_{ZXX} / \chi^{(2)}_{XXZ}$	$\chi^{(2)}_{ZZZ} / \chi^{(2)}_{XXZ}$
Tolcapone	920 nm	+0.71 ± 0.02	+0.99 ± 0.02
	860 nm	+0.74 ± 0.02	+1.10 ± 0.03
	800 nm	+0.83 ± 0.02	+1.24 ± 0.02
Entacapone	920 nm	-	-
	860 nm	-0.6 ± 0.3	-11.0 ± 2.4
	800 nm	+1.2 ± 0.2	+5.9 ± 0.6

Supporting Information Table 3: ratio of non-linear optical susceptibility elements for tolcapone and entacapone obtained by the analysis of the polarization-resolved SSHG experiments at three different wavelengths and at the dodecane/phospholipid/water interface. The values for entacapone at 920 nm were not determined because of a large error due to vanishing SSHG intensity at *s* polarization.

Electronic structure calculations

Density Functional Theory (DFT) calculations were performed using Gaussian09 (rev. D) [2]. The optimized structures for entacapone and tolcapone were obtained at the B3LYP/6-311+G(d,p) level of theory,[13] using the implicit Polarized Continuum Model (PCM) representation for water[14]and the D3 version of Grimme's dispersion[15].
The vertical transition energies were calculated from time-dependent DFT (TD-DFT), [16-18]using the long-range corrected CAM-B3LYP[19] functional. The simulated spectra using a 0.25 eV broadening of the Gaussian lineshape are reported in **Supporting Information Figure 13** together with the experimental ones. The energy axis has been shifted by 0.5 eV to match the experimental spectra. This is due to CAM-B3LYP functional which often overestimates the excitation energies.[20]. In the SSHG experiments we have probed the range from 800 nm to 920 nm, which covers the first excited state of the two compounds. This transition has a small oscillatory strength in the absorption spectra (both experimental and simulated) but show a high second-order non-linear response. This is also showed by the computation of the frequency-dependent hyperpolarizabilities (**Supporting Information Figure 14**). The macroscopic second-order nonlinear susceptibility depends on the hyperpolarizability tensor $\vec{\vec{\beta}}$, the microscopic property that give rise to the non-linear optical response, as:

$$\vec{\vec{\chi}}^{(2)} = \frac{1}{\varepsilon_0} N \left\langle T \right\rangle \vec{\vec{\beta}} \qquad \textbf{(eq. 3)}$$

where $\left\langle T \right\rangle$ is a transformation tensor (averaging over all the orientations) from the molecular to the laboratory frames and *N* is the interfacial density. The theoretical calculation of the hyperpolarizability have been described previously[1] and exploits the Coupled-Perturbed Hartree-Fock procedure. [21,22] For each hyperpolarizability tensor element, a total number of 50 frequencies were calculated in a range centered at the $S_1 \leftarrow S_0$ transition predicted by the TD-DFT calculations. In **Supporting Information Figure 14**, the sum of real and imaginary parts of the hyperpolarizability are reported. It was found that three elements of the hyperpolarizability tensor are non-negligible, namely the β_{zzz}, β_{zzx} and β_{zxx}. The absolute intensity of the hyperpolarizability is in the same

order of magnitude for both tolcapone and entacapone and also the ratio of the hyperpolarizability elements is very similar.
The similarity of the hyperpolarizability tensors and the first excited-state transition dipole moment direction predicted for entacapone and tolcapone allows a direct comparison of the SSHG measurements (**Supporting Information Figure 11**), the latter suggesting a different orientation of the two compounds at the lipid membrane.

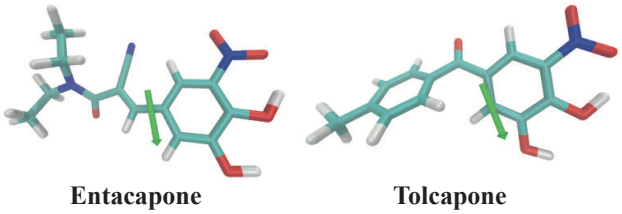

Supporting Information Figure 12: Direction of $S_1 \leftarrow S_0$ transition dipole moment (TDM, in green) of tolcapone (right) and entacapone (left) calculated at the CAM-B3LYP/6-311++G(d,p) level of theory. The two TDM are essentially lying in the same direction with respect to the OCCO group.

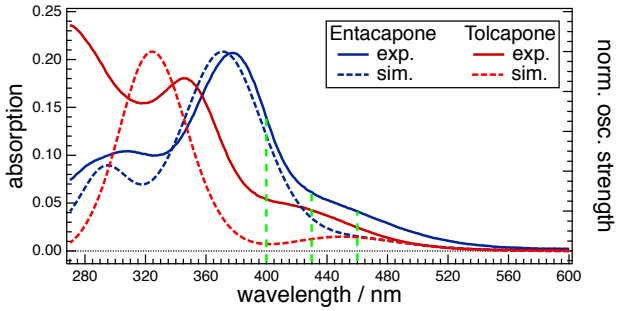

Supporting Information Figure 13: Absorption spectra of tolcapone (red) and entacapone (blue) in water at 10 µM concentration and respective simulated spectra. The dotted vertical lines indicate the wavelengths at which the SSHG signal is in resonance.

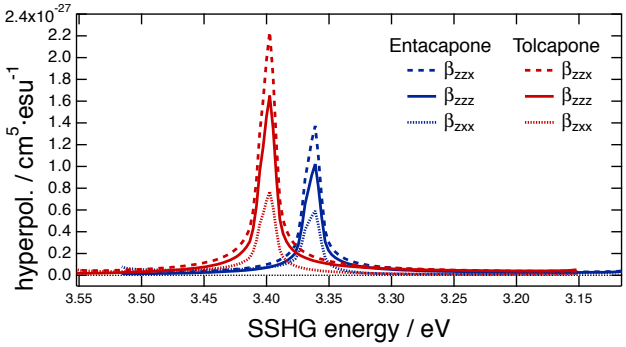

Supporting Information Figure 14: Absolute value of first hyperpolarizability at the resonance frequency of the $S_1 \leftarrow S_0$ transition for tolcapone (red) and entacapone (blue) calculated at the CAM-B3LYP/6-311++G(d,p) level of theory. Only the most intense elements are showed,

the others possessing a negligible contribution to the resonant non-linear response.

Section 6. Results – QCM, SPR and ITC experiments

In our QCM experimental studies, the SLBs used as a model of an internal cell membrane were formed on SiO_2 coated sensors by the vesicle rupture approach. In this approach vesicles can, under specific conditions, initially adsorb onto the SiO_2 surface followed by fusion and rupture of the vesicles to form a lipid bilayer.[23,24] The composition and charge of the formed SLBs resemble that of the vesicles used for preparing the SLBs, i.e. DOPC:DOPE:DOPS with lipid molar ratio 11:15:6, which can be considered as an approximate model of an intracellular membrane.[25] The methodology used in the deposition of the SLBs on the QCM SiO_2 coated sensors follows a well-established pathway and provided with great reproducibility good quality SLBs (**Supporting Information Figure 15**).

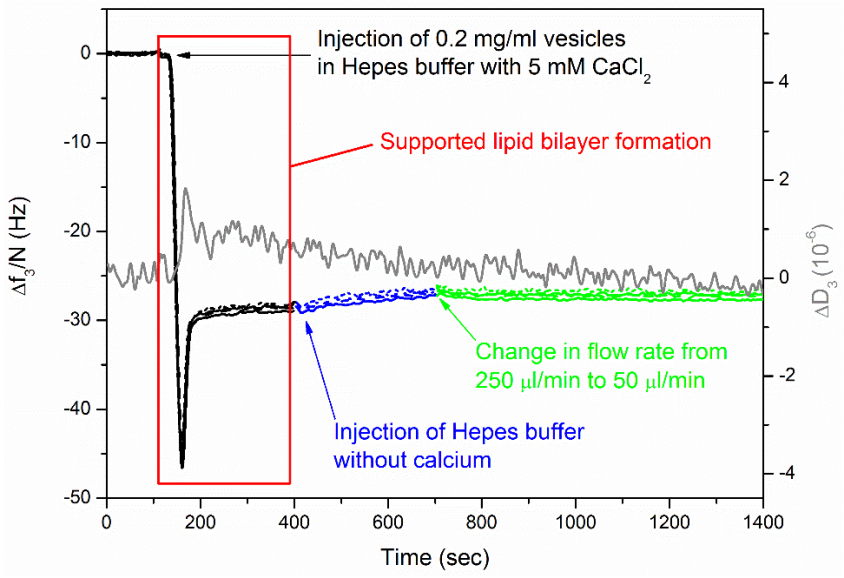

Supporting Information Figure 15: SLB formation for QCM measurements was verified and monitored by simultaneously recording the frequency change and dissipation change at the 3rd , 5th, 7th, and 9th overtones during injection of DOPC:DOPE:DOPS vesicles.

A simpler model membrane system consisting of pure DOPC were used for SPR studies due to the difficulty of spreading more complex lipid compositions as a bilayer on the SiO_2 coated SPR sensors.

For the three systems, ADOMET, COMT, and (COMT+ADOMET) the QCM frequency responses of the third overtone after 8 minutes of interaction with the DOPC:DOPE:DOPS lipid bilayer were measured to be −1.58 ± 0.12 Hz, −0.54 ± 0.13 Hz and −3.58 ± 0.34 Hz, respectively (**Figure 3C, main manuscript**). Similarly, the SPR responses for the DOPC system were 4.5 ± 1.1 m° (ADOMET), ~0 m° (COMT) and 10.5 ± 2.0 m° (COMT+ADOMET) (**Supporting Information Figure 15**). The ANOVA statistical analysis showed that the sum of the QCM responses measured for COMT and ADOMET and the QCM response measured for COMT+ADOMET, as well as the SPR responses measured for ADOMET and COMT+ADOMET were both significantly different at a significance level of 0.01. The QCM and SPR measurements are well

in line with each other showing that the mixture of (COMT+ADOMET) containing the holo form of COMT has a stronger interaction with lipid membranes in comparison to plain COMT, i.e. the apo form of the enzyme.

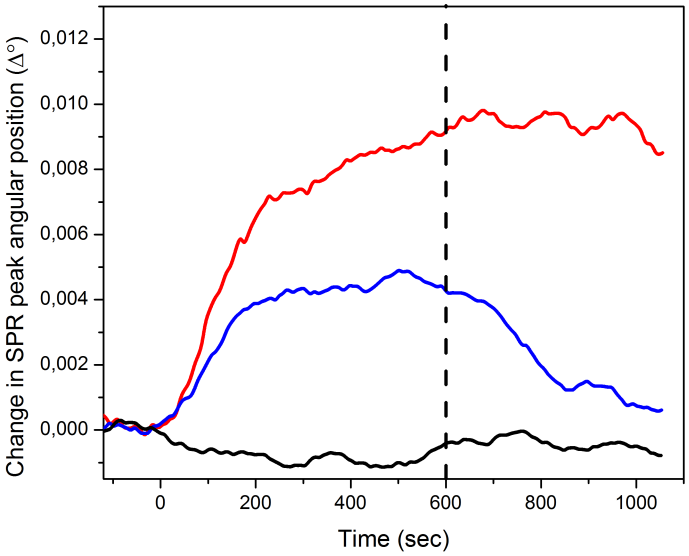

Supporting Information Figure 16: SPR signal responses measured during interaction of 2 mM ADOMET (blue line), 40 μM COMT (black line), and a mixture of 40 μM COMT + 2 mM ADOMET (red line) with a DOPC lipid bilayer. Samples were injected at t = 0 min and allowed to interact with the bilayer for 10 minutes, whereafter the running buffer was injected (dashed vertical line).

Supporting Information Figures 17-19 show the heat flow curves and the titration curves measured with ITC during repeat injections of 5 µL of DOPC:DOPE:DOPS vesicles into 0.2 mM ADOMET, 4 µM COMT and (4 µM COMT+0.2 mM ADOMET), respectively. **Supporting Information Table 4** summarizes the parameters extracted by fitting the titration curves for ADOMET, COMT and (COMT+ADOMET) with the AFFINImeter analysis software. (**Supporting Information Table 4** and **Supporting Information Figure 20** shows the thermodynamic parameters obtained from the data fitting procedure. The ITC measurements shows that the system containing the holo form of the protein (COMT+ADOMET) exhibit a higher affinity (K_D = 45 ± 16 µM) towards the lipid bilayer in the DOPC:DOPE:DOPS vesicles compared to the apo form of the protein (COMT, K_D = 106 ± 65 µM) (**Supporting Information Table 4** and **Figure 3C in main manuscript**).

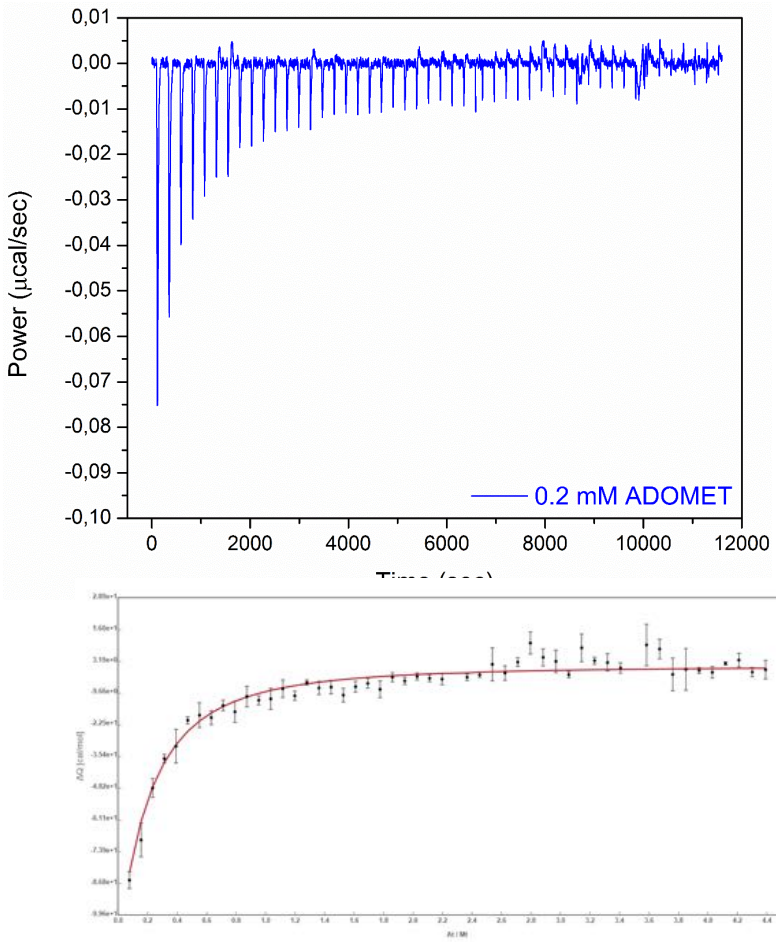

Supporting Information Figure 17. Upper panel: Heat flow curve measured during repeat 5 µL injections of DOPC:DOPE:DOPS vesicles (total lipid concentration 5 mM) into 0.2 mM ADOMET. Lower panel: Titration curve obtained by determining the area of the injection heat pulses in the upper panel (black dots), including data fit to extract thermodynamic parameters (red line).

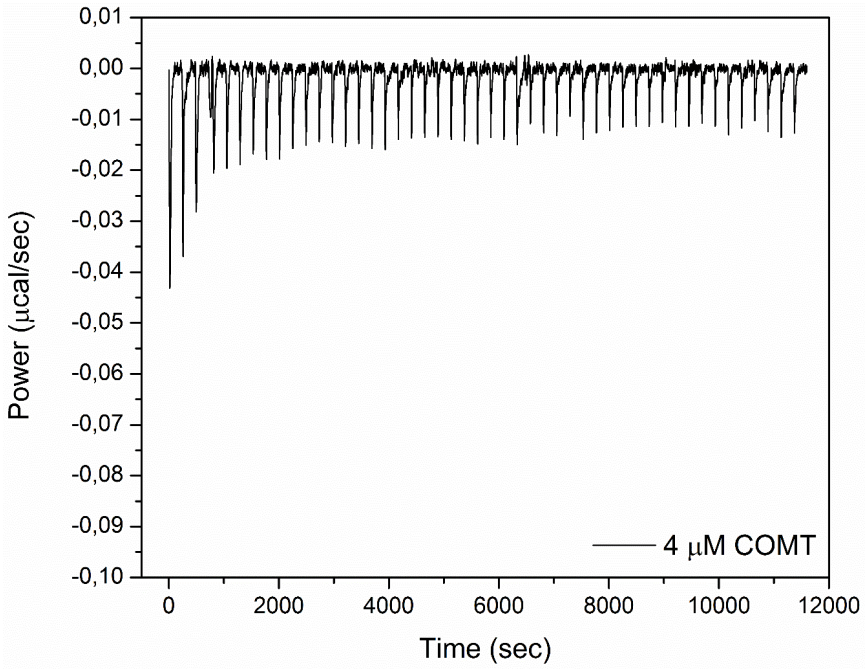

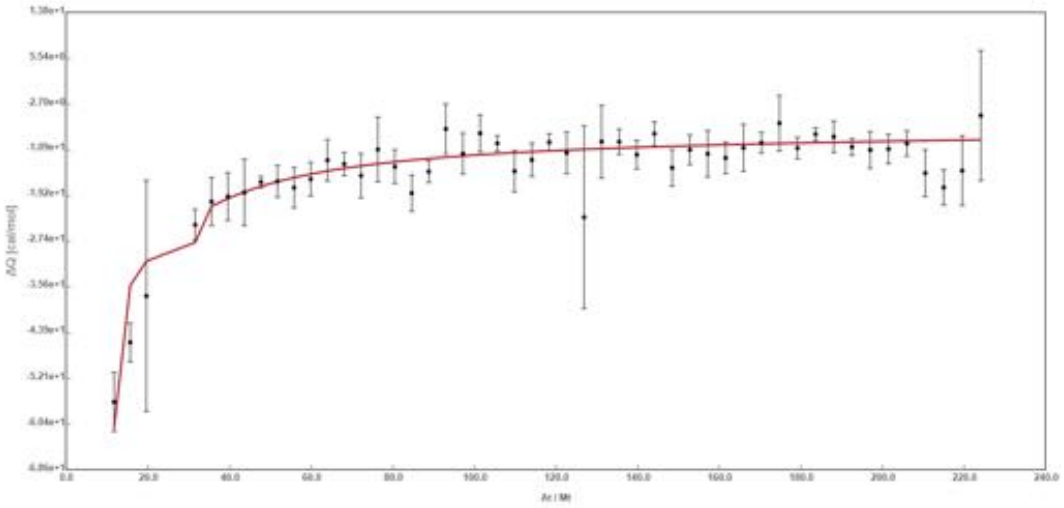

Supporting Information Figure 18: Upper panel: Heat flow curve measured during repeat 5 µL injections of DOPC:DOPE:DOPS vesicles (total lipid concentration 5 mM) into 4 µM COMT. Lower panel: Titration curve obtained by determining the area of the injection heat pulses in the upper panel (black dots), xincluding data fit to extract thermodynamic parameters (red line).

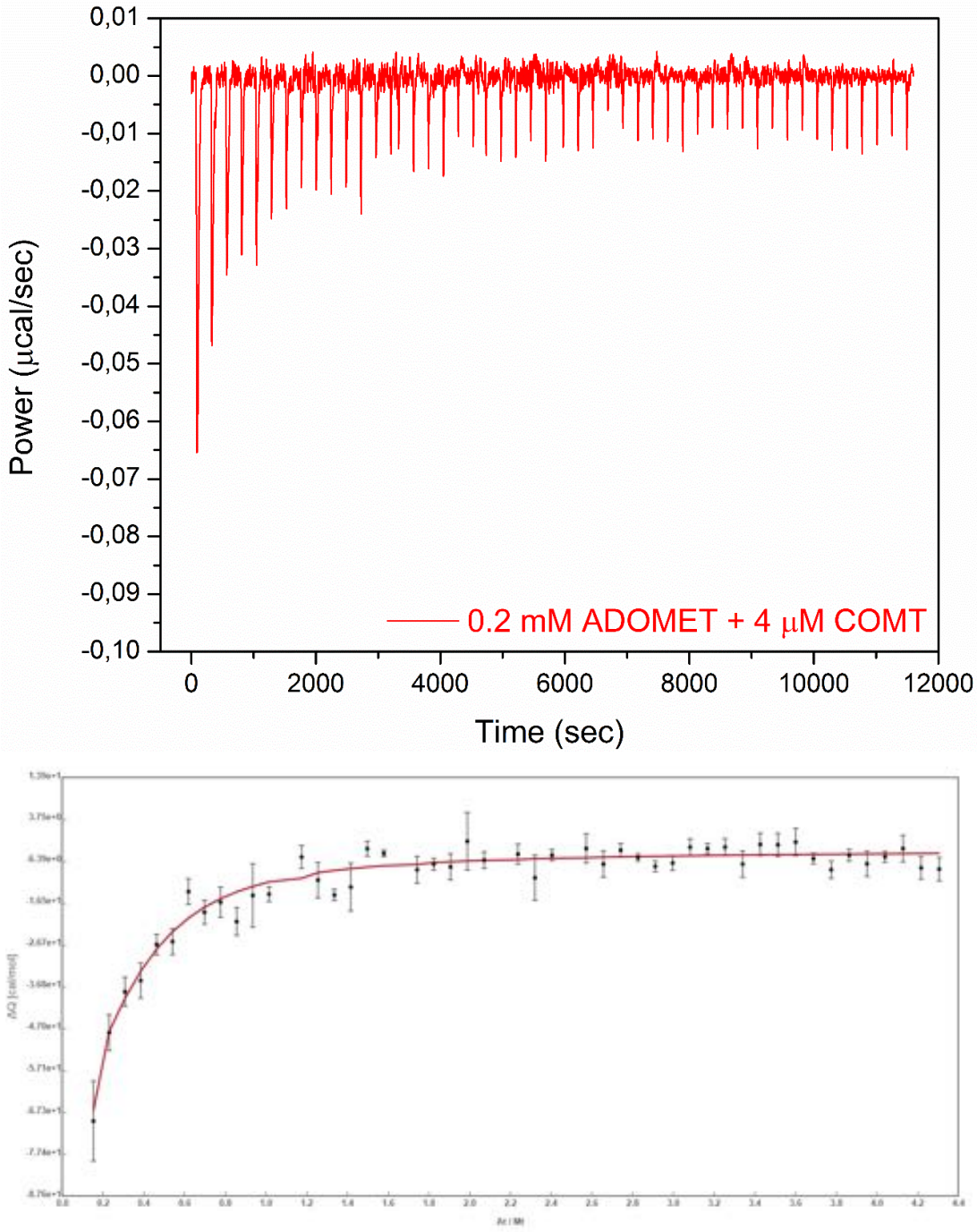

Supporting Information Figure 19: Upper panel: Heat flow curve measured during repeat 5 µL injections of DOPC:DOPE:DOPS vesicles (total lipid concentration 5 mM) into 4 µM COMT+0.2 mM ADOMET. Lower panel: Titration curve obtained by determining the area of the injection heat pulses in the upper panel (black dots), including data fit to extract thermodynamic parameters (red line).

Supporting Information Table 4: Summary of parameters extracted by fitting ITC measurements.

	Temp [K]	χ^2	ΔH_{dil} [cal/mol]	r_M	K_A [M^{-1}]	K_D [M]	ΔH [cal/mol]	$T \cdot \Delta S$ [cal/mol]	ΔG [cal/mol]
COMT	310.15	8.587e-1	-1.003e+1 ± 9.69e-1	4.499e-1 ± 1.47e+1	9.394e+3 ± 5.76e+3	1.064e-4 ± 6.52e-5	-3.513e+3 ± 1.23e+5	2.125e+3 ± 1.23e+5	-5.638e+3 ± 3.78e+2
ADOMET	310.15	1.770e+0	1.421e+0 ± 6.58e-1	1.367e-2 ± 1.01e-1	1.073e+4 ± 2.76e+3	9.319e-5 ± 2.40e-5	-3.415e+3 ± 2.40e+4	2.305e+3 ± 2.40e+4	-5.720e+3 ± 1.58e+2
COMT +ADOMET	310.15	1.699e+0	-4.824e+0 ± 5.97e-1	2.600e-1 ± 1.03e-1	2.198e+4 ± 7.84e+3	4.549e-5 ± 1.62e-5	-1.246e+2 ± 6.01e+1	6.037e+3 ± 2.28e+2	-6.162e+3 ± 2.20e+2

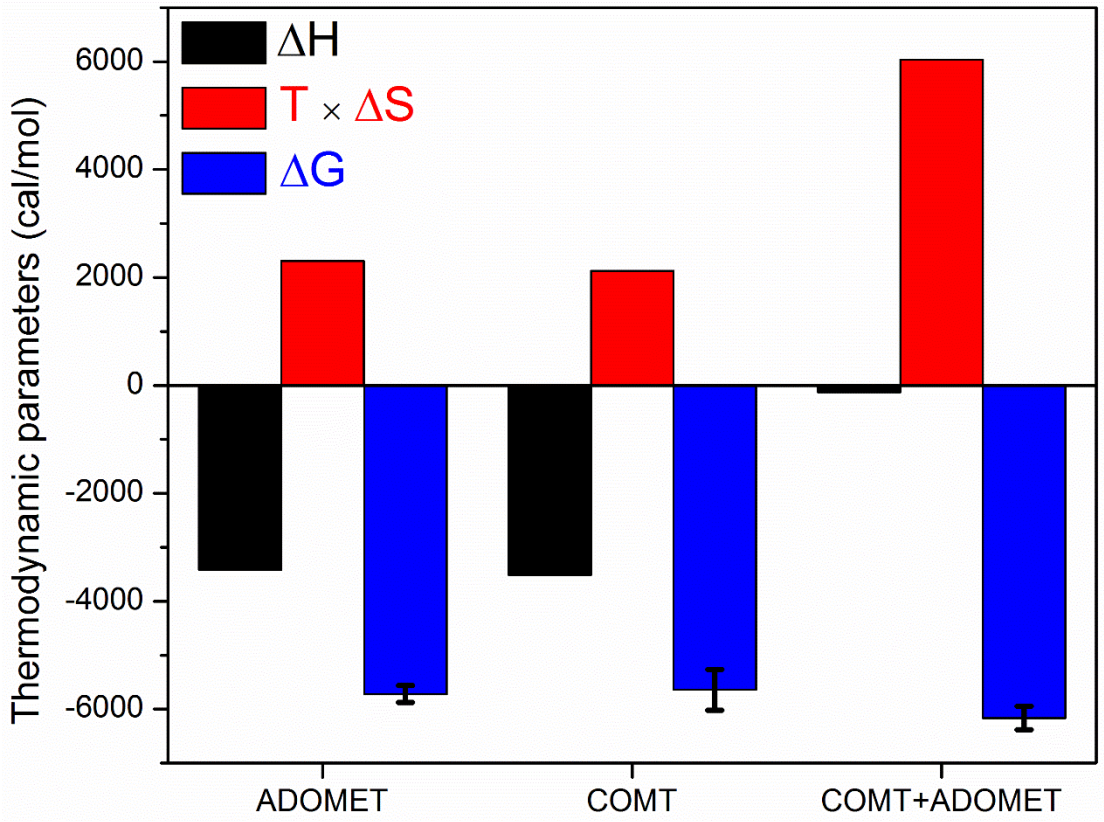

Supporting Information Figure 20: Graphical representation of the thermodynamic parameters obtained by fitting ITC measurements.

Section 7. Data mining results

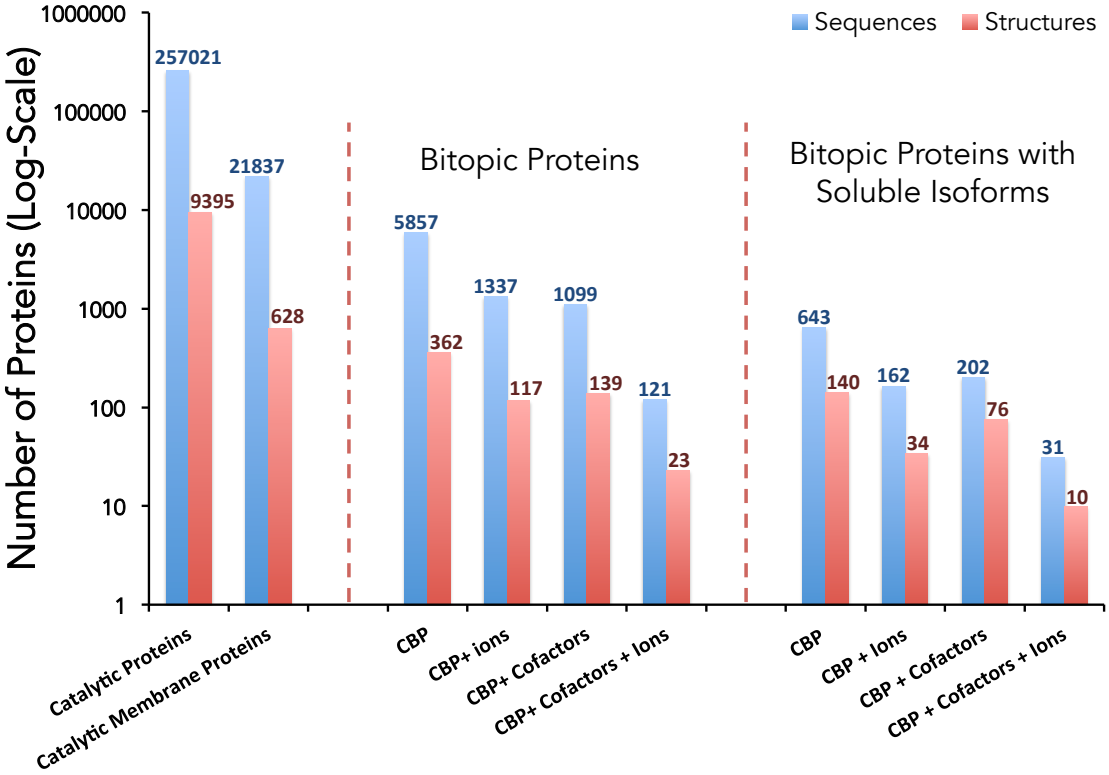

Supporting Information Figure 21: Number of sequences and sequences where the structure of the catalytic domain is known, for bitopic proteins and bitopic proteins that also possess a water-soluble isoform, relative to the total number of catalytic proteins and catalytic membrane proteins sequenced.

References

(1) Bayly, C. I.; Cieplak, P.; Cornell, W.; Kollman, P. A. *J. Phys Chem.* **2002**, *97* (40), 10269.
(2) Knox, J. E.; Hratchian, H. P.; Cross, J. B.; Bakken, V.; Adamo, C. *Gaussian 03, Revision C. 02. Gaussian*; Inc.: Wallingford, 2004.
(3) Wang, J.; Wang, W.; Kollman, P. A.; Case, D. A. *Journal of Molecular Graphics and Modelling* **2006**, *25* (2), 247.
(4) Orłowski, A.; St-Pierre, J.-F.; Magarkar, A.; Bunker, A.; Pasenkiewicz-Gierula, M.; Vattulainen, I.; Róg, T. *J. Phys Chem. B* **2011**, *115* (46), 13541.
(5) Tsuji, E.; Okazaki, K.; Isaji, M.; Takeda, K. *Journal of Structural Biology* **2009**, *165* (3), 133.
(6) Palma, P. N.; Rodrigues, M. L.; Archer, M.; Bonifacio, M. J.; Loureiro, A. I.; Learmonth, D. A.; Carrondo, M. A.; Soares-da-Silva, P. *Mol Pharmacol* **2006**, *70* (1), 143.
(7) Hub, J. S.; de Groot, B. L.; van der Spoel, D. *J Chem Theory Comput* **2010**, *6* (12), 3713.
(8) Licari, G.; Brevet, P.-F.; Vauthey, E. *Physical Chemistry Chemical Physics* **2016**, *18* (4), 2981.
(9) Fedoseeva, M.; Letrun, R.; Vauthey, E. *J. Phys Chem. B* **2014**, *118* (19), 5184.
(10) Brevet, P. F. *Surface second harmonic generation*; 1997.
(11) Nagatani, H.; Piron, A.; Brevet, P.-F.; Fermín, D. J.; Girault, H. H. *Langmuir* **2002**, *18* (17), 6647.
(12) Wang, H.; Borguet, E.; Eisenthal, K. B. *J. Phys Chem. B* **1998**, *102* (25), 4927.
(13) Lee, C.; Yang, W.; Parr, R. *Phys. Rev., B Condens. Matter* **1988**, *37* (2), 785.
(14) Marenich, A. V.; Cramer, C. J.; Truhlar, D. G. *J. Phys Chem. B* **2009**, *113* (18), 6378.
(15) Grimme, S.; Antony, J.; Ehrlich, S.; Krieg, H. *J. Chem. Phys.* **2010**, *132* (15), 154104.
(16) Bauernschmitt, R.; Ahlrichs, R. *Chemical Physics Letters* **1996**, *256* (4-5), 454.
(17) Stratmann, R. E.; Scuseria, G. E.; Frisch, M. J. *The Journal of Chemical Physics* **1998**, *109* (19), 8218.
(18) Scalmani, G.; Frisch, M. J.; Mennucci, B.; Tomasi, J.; Cammi, R.; Barone, V. *The Journal of Chemical Physics* **2006**, *124* (9), 94107.
(19) Yanai, T.; Tew, D. P.; Handy, N. C. *Chemical Physics Letters* **2004**, *393* (1-3), 51.
(20) Fukuda, R.; Ehara, M. *J. Chem. Phys.* **2012**, *136* (11), 114304.
(21) Sekino, H.; Bartlett, R. J. *The Journal of Chemical Physics* **1986**, *85* (2), 976.
(22) Rice, J. E.; Handy, N. C. *The Journal of Chemical Physics* **1991**, *94* (7), 4959.
(23) Cho, N.-J.; Frank, C. W.; Kasemo, B.; Höök, F. *Nat Protoc* **2010**, *5* (6), 1096.
(24) Keller, C. A.; Kasemo, B. *Biophysical Journal* **1998**, *75* (3), 1397.
(25) van Meer, G.; Voelker, D. R.; Feigenson, G. W. *Nature Reviews Molecular Cell Biology* **2008**, *9* (2), 112.